

ARTICLES

Dielectric Friction and Rotational Diffusion of Hydrogen Bonding Solutes

Kathy Wiemers and John F. Kauffman*

Department of Chemistry, University of Missouri—Columbia, 123 Chemistry Building, Columbia, Missouri 65211

Received: April 6, 1999; In Final Form: September 17, 1999

Rotational diffusion times (τ_r) of 4-(hydroxymethyl)stilbene (HMS) have been measured as a function of temperature in seven *n*-alcohols from ethanol through octanol. Stokes–Einstein–Debye plots (τ_r versus η/T , η = viscosity) indicate substantial friction in excess of that predicted by the Stokes–Einstein–Debye model for mechanical friction. Comparison of HMS with diphenylbutadiene (DPB), a solute of similar size and shape but without the hydroxyl group, suggests that hydrogen bonding interactions influence the HMS rotational diffusion time. Hydrogen bonding is modeled as dielectric friction using the longest solvent Debye relaxation time in the zero-frequency limiting form of the Nee–Zwanzig equation. The longest Debye relaxation time of alcohols is associated with rotational motion of solvent molecules in hydrogen bonded clusters and reflects the time scale for breaking of hydrogen bonds. The HMS results are well represented when the dielectric friction contribution is added to the DPB data. Agreement between model and data suggests that hydrogen bonding is responsible for the additive contribution of dielectric friction to the rotational diffusion time of HMS in *n*-alcohols.

I. Introduction

Studies of solute rotational time correlation functions have been widely used to characterize solvent–solute friction,^{1–29} and yet no universally applicable model for rotational dynamics has been identified. The Debye small step diffusion model casts the rotational time correlation function as an exponential characterized by the rotational diffusion time, τ_r .³⁰ The Stokes–Einstein–Debye (SED) model considers solvent friction arising from viscous drag on the solute molecule.^{6,9,25} In this model, τ_r is a linear function of η/T with slope V_p/k (η = solvent viscosity, T = temperature, V_p = solute volume, and k = Boltzmann constant; $k = 0.0138$ [centipoise \AA^3]/[ps Kelvin]). This model has been successfully applied to rotational diffusion of large solute molecules in regular liquids.^{9,25} However, when the size of the solute molecule approaches the size of the solvent, the slope of the plot changes and corrections must be applied to the SED formula to account for solvent “molecularity” and solute shape.^{13,31} This model works well when frictional interactions are predominantly collisional, repulsive interactions. The repulsive friction is referred to as mechanical friction because it is largely determined by solute size and shape.

The situation is more complicated in polar solvent–solute systems because dielectric friction contributes to the measured rotational diffusion time. Early theories of dielectric friction described a contribution from the solvent reaction field that reflects the torque on the solute molecule due to the reaction field induced by the solute.^{2,4,5,21,22,29} Subsequently, several theories on dielectric friction have been published,^{2,5,21,29} and

all of the theories assume that dielectric friction for a spherical solute molecule results in an additive contribution to τ_r . When the solvent dielectric constant exceeds 10 and in the zero frequency limit, the additive contribution, τ_{DF} , scales with solute dipole moment (μ) and solvent dielectric constant (ϵ) according to the Nee–Zwanzig expression,^{2,5}

$$\frac{\mu^2}{kT\rho^3} \frac{\epsilon - 1}{\epsilon_0(2\epsilon + 1)^2} \tau_d \quad (1)$$

where ρ is the radius of the cavity in the dielectric continuum that contains the solute, kT is the thermal energy, ϵ_0 is the permittivity of free space, and τ_d is the Debye relaxation time of the solvent. This model assumes that the solute is well represented as a point dipole at the center of the cavity. The additive correction can be viewed simplistically in the framework of the Langevin equation,^{30,32} which provides a relationship between the reduced friction coefficient (ζ) and the time integral of the random torque (Γ) autocorrelation function

$$\zeta = \frac{1}{mkT} \sum_0^{\infty} \langle \Gamma(t)\Gamma(0) \rangle dt$$

Separating the torque into a sum of attractive and repulsive contributions, the integral of the autocorrelation function includes an attractive contribution, a repulsive contribution, and a cross term reflecting correlation (or coupling) between the attractive and repulsive contributions. The latter will only be significant near the repulsive barrier. When the cross term is negligible, the friction is the sum of an attractive and a repulsive

* To whom correspondence should be addressed. E-mail: kauffmanj@missouri.edu.

contribution. Within this framework, attractive contributions to solvent–solute friction may result from a variety of attractive interactions. Proper theoretical analysis of the attractive contribution to solvent–solute friction requires a generalized Langevin equation in order to account for the time lag between the solute velocity and the frictional force it experiences resulting from its reaction field. The frequency-dependent dielectric function, characterized by the Debye relaxation time, offers a convenient means of parametrizing the molecular response within a continuum model. Note, however, that while decoupling of the attractive and repulsive contributions to the friction is convenient for interpretation of experimental data, its validity cannot be considered a forgone conclusion.^{33–35}

In this paper, we examine rotational diffusion of two solute molecules, diphenylbutadiene (DPB) and 4-(hydroxymethyl)-stilbene (HMS), in a series of alcohols in order to examine attractive and repulsive contributions to the rotational diffusion time. Experimental rotational diffusion times (RDTs) for the two solutes exhibit large differences in the alcohols. Comparison of the results to a modified SED model indicates that the difference between the HMS and DPB results are not the result of differences in solute size and shape. The observed differences between the results for DPB and HMS are modeled with the addition of an attractive contribution to the DPB results. The results suggest that specific hydrogen bonding interactions between HMS and the solvent are responsible for significant solvent friction.

II. Experimental Section

trans-4-Stilbenemethanol (HMS) from Aldrich was used as obtained. Anisotropies were measured in a series of *n*-alcohols. Ethanol, 1-propanol, and 1-butanol were used as obtained. The higher alcohols, 1-pentanol, 1-hexanol, 1-heptanol, and 1-octanol were purchased from ICN Biochemical, Inc. and were fractionally distilled over ground 4 Å molecular sieves. Before each experiment, the 1 cm quartz cuvettes were soaked in a Nochromix solution for 3 min, rinsed with deionized water three times, and then rinsed with absolute ethanol. Sample preparation for the DPB measurements has been reported elsewhere.⁶

Anisotropy measurements were initially taken using a commercial spectrophotometer. However, photochemistry of stilbene derivatives can result in substantial temporal variations in the signal, and this contributed to unacceptably large uncertainties in the measured anisotropies. To overcome this problem, we have constructed a fluorimeter that uses the sample fluorescence as a reference and collects signal and reference simultaneously. A Xenon arc lamp is used as the light source for anisotropy measurements. The lamp was focused into a calibrated monochromator set to 298 nm. The beam was focused through a polarizer and into the sample compartment. Anisotropies were measured over a temperature range of 10–60 °C. A thermostated cuvette holder of our own design controlled the temperature to within ±0.1 °C of the set temperature. The fluorescence signal was collected at a right angle to the plane of the excitation polarization with a *f*/4 collimating lens and directed through a computerized, step-motor-controlled, wide-aperture, Glan-Taylor polarizer and a 370 ± 5 nm band-pass filter. Fluorescence photons were detected by a cooled Hamamatsu R2809U-11 microchannel plate PMT using photon counting electronics. A second PMT/monochromator channel (T-format) detected the 370 nm fluorescence from the sample, and this channel was used as a reference. Signal and reference counts were collected simultaneously on two independent channels of a programmable 10-channel counter (Computer Boards, Inc. model CIO-CTR10).

Two additional counters were used to control the polarizer step motor, and a fifth channel was used along with a rotary encoder to ensure that the polarizer moved through the correct angle when switching between parallel and perpendicular polarizations. A shutter in the excitation beam allowed subtraction of background counts, and minimized sample exposure during inactive periods. All hardware manipulations, data collection, and anisotropy calculations are implemented with a program of our own design using the HP VEE 2.1 visual programming language. The background-corrected signal counts are divided by the background-corrected reference counts for each measurement to correct for signal intensity fluctuations. Each reported anisotropy is the average of five measurements. A typical standard deviation is 0.002. The *G* factor³⁶ was measured prior to experiments, and a *G* factor correction is also included in the anisotropy calculation.

Rotational correlation times were calculated from static anisotropies using the Perrin equation³⁶

$$\tau_r = \tau_f \frac{r}{r_0 - r}$$

where τ_f is the fluorescence lifetime and r_0 is the limiting anisotropy. The Perrin equation is valid when the fluorescence decay and the anisotropy decay are single exponential. Fluorescence lifetimes were measured by the time correlated photon counting method using instrumentation which has been described previously.^{37,38} Magic angle fluorescence decays are well fit by single-exponential model functions using the iterative reconvolution method. DPB fluorescence decay results have been published previously,³⁷ and a detailed discussion of HMS fluorescence decays and isomerization rates will be presented in another paper.³⁹ Anisotropy decays for diphenylpolyenes have been widely demonstrated to be single exponential, as is expected for prolate rotors whose transition dipole is aligned with the long molecular axis. The value of r_0 was determined by measuring the anisotropy of HMS in glycerin at 0 °C and was found to be 0.34 ± 0.01 . Previous measurements of DPB in glycerin give an r_0 value of 0.39 ± 0.01 .⁶ The anisotropy (r) is calculated using the standard formula,³⁶

$$r = \frac{I_{\text{pl}} - GI_{\text{pp}}}{I_{\text{pl}} + 2GI_{\text{pp}}}$$

where I_{pl} and I_{pp} are the parallel and perpendicular fluorescence intensities, respectively. Rotational correlation times as short as a few picoseconds can be determined from static anisotropies because the diphenylpolyenes have short fluorescence lifetimes due to excited-state isomerization. The dipole moment of HMS was measured using an instrument of our own design, which has been described previously.^{40,41}

III. Results

Experimental rotational diffusion times for HMS and DPB are compared in Figure 1 for two of the seven solvents examined in this study. Additional figures are available as Supporting Information. The behavior of each solute in each solvent is characterized by a linear dependence of τ_r on η/T as predicted by the SED model. The ethanol data give the best linear regression fit for each solute (correlation coefficient $R = 0.99$), and the octanol data give the worst fit ($R = 0.97$). HMS has a van der Waals volume of $V_{\text{HMS}} = 210 \text{ \AA}^3$ and DPB has a van der Waals volume of $V_{\text{DPB}} = 208 \text{ \AA}^3$. Within the SED model, the slopes of the plots of τ_r vs η/T should be essentially identical.

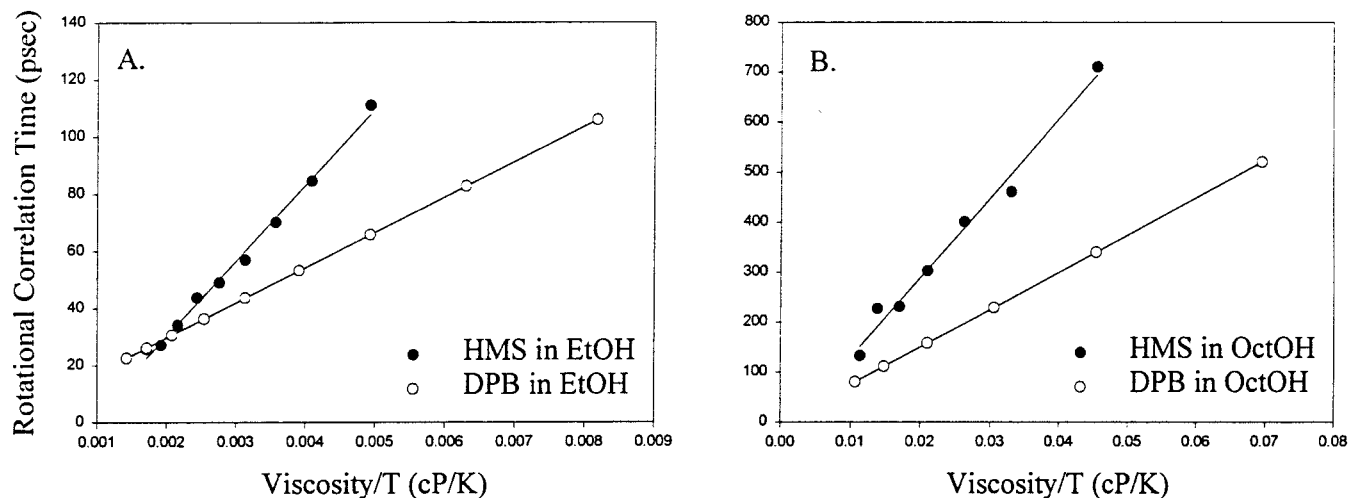
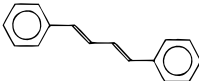
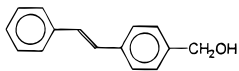


Figure 1. Representative measured rotational diffusion times of HMS and DPB in (A) ethanol and (B) octanol. The points are measured values, and the lines are linear regressions of the measurements. All DPB results are highly linear ($R = 0.99$). Ethanol and octanol give the best and worst correlation coefficients, respectively, in the linear regression analysis of the HMS data.

TABLE 1: Properties of HMS and DPB^a

	DPB	HMS
		
molar mass	206 g/mol	210 g/mol
inertial moments		
I_A ($\times 10^{-40}$ g/cm ²)	328.5	374.9
I_B	5693.5	4938.9
I_C	6021.6	5305.5
van der Waals volumes	208 Å ³	210 Å ³
ellipsoid parameters		
long axis	16.3 Å	15.8 Å
short axis	4.93 Å	5.04 Å
axial ratio	3.31 Å	3.14 Å
f_{stick}	2.65	2.48
f_{slip}/f_{stick}	0.507	0.479
radiative lifetime	7.7×10^8 s ⁻¹	8.1×10^8 s ^{-1b}
τ_r (hexane, 25 °C)	28 ps	24 ps
τ_r (ethanol, 25 °C)	47 ps	70 ps
τ_f (hexane, 25 °C)	511 ps	130 ps
τ_f (ethanol, 25 °C)	74 ps	80 ps

^a These properties reflect the size and shape of the two solutes examined in this study. Solvent dependent, room-temperature fluorescence lifetimes and rotational diffusion times reflect the influence of solvent on rotational diffusion and configurational isomerization. ^b The radiative lifetime of HMS was determined from integrated absorption and emission spectra using the Strickler–Berg⁴⁸ method.

However, the slopes for each solute vary with solvent, and in each of the C2 through C8 *n*-alcohols, the HMS slope is observed to be larger than the DPB slope by a factor of 2.8 on average. One possible explanation for the observation is that the rotational diffusion times of the solutes are particularly sensitive to the solute shape as characterized by moments of inertia and axial ratios. We have compared our experimental results with calculated values for rotational correlation times using a modified form of the SED model⁶ that includes a shape factor (f_{stick}) and a boundary condition factor (C),

$$\tau_r = \frac{\eta V}{kT} f_{stick} C + \tau_0 \quad (2)$$

The solutes are modeled as prolate ellipsoids, since rotation about the long axis is fast compared with rotations around perpendicular axes. In this case, f_{stick} depends only on the ratio of the solute major and minor axes. (See ref 6 and references therein for details of the calculation.) Values for f_{stick} and other important properties of these two solutes are compared in Table

1. Solvent and solute van der Waals volumes have been estimated using the group contribution method of Bondi.⁴² Solute inertial moments and long axes have been found using semiempirical structural optimization (HyperChem). The ellipsoid minor axes have been estimated from the long axis and the van der Waals volume by requiring the ellipsoid volume to equal the van der Waals volume.^{9,43} f_{stick} was calculated using eq 2 of ref 6. Because the properties that characterize the size and shape of the solutes are very similar, the shape factors for HMS and DPB are similar and cannot account for the differences in the observed behavior of these two solutes. The remaining factor in eq 2 that influences the slope of the plots in Figure 1 is the boundary condition factor. We have calculated the boundary condition factors for HMS and DPB in each of the solvents from the linear regression slopes of the experimental data using eq 2 along with calculated temperature-dependent viscosities and the solute parameters given in Table 1. These “measured” boundary condition factors are reported in Tables 2 and 3 for DPB and HMS, respectively.

TABLE 2: DPB Boundary Condition Factors^a

alcohol	measured	DKS	modified DKS
ethanol	0.309	0.155	0.429
propanol	0.254	0.100	0.426
butanol	0.239	0.091	0.420
pentanol	0.163	0.079	0.369
hexanol	0.199	0.070	0.642
heptanol	0.174	0.054	0.435
octanol	0.187	0.051	0.461

^a The table indicates values of C determined from regression values for lines which characterize data or models. DKS and m-DKS models: the fit is to the values determined versus temperature and then plotted versus η/T . Data: the values are fits to the data versus measured temperatures and calculated viscosities. The average correlation coefficient for linear fits to the DKS model for both solutes is $R^2 = 0.98 \pm 0.01$, and the minimum correlation coefficient is 0.95. The average correlation coefficient for linear fits to the modified DKS model for both solutes is $R^2 = 0.995 \pm 0.006$, and the minimum correlation coefficient is 0.98. The average correlation coefficient for linear fits to the data for both solutes is $R^2 = 0.99 \pm 0.01$, and the minimum correlation coefficient is 0.97. Standard errors from regression slopes indicate relative uncertainties in measured values of less than 1%.

TABLE 3: HMS Boundary Condition Factors^a

alcohol	measured	DKS	modified DKS
ethanol	0.70 ± 0.02	0.165	0.381
propanol	0.68 ± 0.03	0.115	0.378
butanol	0.64 ± 0.03	0.109	0.372
pentanol	0.56 ± 0.02	0.096	0.330
hexanol	0.61 ± 0.02	0.090	0.576
heptanol	0.54 ± 0.01	0.063	0.338
octanol	0.42 ± 0.02	0.059	0.413

^a The table indicates values of C determined from regression values for lines which characterize data or models. DKS and m-DKS models: the fit is to the values determined versus temperature and then plotted versus η/T . Data: the values are fits to the data versus measured temperatures and calculated viscosities. The average correlation coefficient for linear fits to the DKS model for both solutes is $R^2 = 0.98 \pm 0.01$, and the minimum correlation coefficient is 0.95. The average correlation coefficient for linear fits to the modified DKS model for both solutes is $R^2 = 0.995 \pm 0.006$, and the minimum correlation coefficient is 0.98. The average correlation coefficient for linear fits to the data for both solutes is $R^2 = 0.99 \pm 0.01$, and the minimum correlation coefficient is 0.97. Uncertainties in measured values are standard errors from the linear regressions.

f_{stick} corrects the SED model for nonspherical solute shape assuming the stick boundary condition. Thus, under stick boundary conditions the boundary condition factor has a value of $C = 1$. Under slip conditions, C has a value equal to $f_{\text{slip}}/f_{\text{stick}}$. Hu and Zwanzig⁴⁴ have demonstrated that $f_{\text{slip}}/f_{\text{stick}}$ depends on the axial ratio, A , and have tabulated values of $f_{\text{slip}}/f_{\text{stick}}$ for both prolate and oblate rotors. We have fit their prolate rotor results to a five-parameter sigmoid of the form

$$\frac{f_{\text{slip}}}{f_{\text{stick}}} = \frac{C1}{\left[1 - \exp\left(-\frac{A - C4}{C2}\right)\right]^{C3}} + C5$$

in order to accurately interpolate (i.e., within 1% of the tabulated values) between tabulated data points. (For prolate rotors, $C1 = 0.93$, $C2 = 1.28$, $C3 = 16.66$, $C4 = -1.87$, and $C5 = -0.19$; for oblate rotors, $C1 = 1.05$, $C2 = 1.28$, $C3 = 11.05$, $C4 = -1.24$ and $C5 = -0.20$.) Values of $f_{\text{slip}}/f_{\text{stick}}$ thus determined are given in Table 1. The boundary condition factors tabulated in Tables 2 and 3 can be compared with the stick prediction ($C = 1$) and the slip predictions ($C = 0.507$ for DPB and $C = 0.479$ for HMS) for each solute. DPB exhibits a subslip boundary condition in each of the solvents. On the other hand,

HMS exhibits a boundary condition between the stick and slip limits in all solvents except octanol. Clearly HMS experiences greater friction than DPB in each solvent. The fact that HMS is more polar than DPB suggests that dielectric friction is involved. However, the boundary condition factor depends on both solvent and solute properties in a complex manner, and before we consider dielectric friction, we wish to examine the sensitivity of the hydrodynamic boundary condition factor to solute properties. We choose to examine this issue by calculating boundary condition factors using two related quasihydrodynamic models.

IV. Calculation of the Boundary Condition Factor

The Dote–Kivelson–Schwartz (DKS)¹³ model for the boundary condition factor has been shown to represent the transition from slip to stick well for regular solutions.²⁵ A succinct discussion of the model can be found in ref 6. Briefly, this model relates the boundary condition factor to the amount of free space available to the solute molecule. The free space increases as the solute becomes small compared to the solvent. The free space also depends on ΔV , “the smallest volume of free space per solvent molecule”, a quantity that can be related to solvent thermodynamic properties using regular solution theory. Thus, the boundary condition depends on both solvent and solute volumes as well as temperature. We have calculated the predicted rotational diffusion times using the modified SED model with DKS boundary condition (referred to as the DKS model) for each solute in each alcohol over a range of temperatures. We find that the results are nearly linear in η/T over the temperature range of this study. To compare the predicted results with measured results, we characterize the predicted boundary condition for each solute in each alcohol by calculating C from the linear regression slopes of plots of predicted τ_r 's versus η/T for each alcohol using eq 2. The results are tabulated in Tables 2 and 3. On average the DKS model underestimates the measured boundary condition factors for DPB by a factor of about 2.5, and it underestimates the HMS boundary condition by a factor of 5.5. In a previous report, we have suggested that the DKS model must be modified for alcohols to account for temperature-dependent changes in free space due to solvent hydrogen bonding.⁶ In this modification of the DKS model, we replace the calculated ΔV parameter by the empirical term $\Delta V = V_m - V_{\text{vdw}}$, where V_m is the solvent molar volume and V_{vdw} is the van der Waals volume of the solvent. These calculations have also been performed for HMS. The results for both HMS and DPB are found to be highly linear in η/T , and the boundary conditions determined from the linear regression slopes using eq 2 are also given in Tables 2 and 3. The results of the DKS and modified DKS (hereafter referred to as m-DKS) calculations for DPB differ slightly from our previously reported results. In the previous study, we used both van der Waals and molar volumes in calculating parameters in the boundary condition factor, C . In the present study, all volumes are van der Waals volumes with the exception of the molar volume used in calculating ΔV . The calculations in the present study are therefore completely self-consistent with respect to the measures used to characterize solvent and solute volume. Molar volumes are estimated from critical constants of the alcohols using the modified Rackett technique.⁴⁵ The anomalous results for hexanol in Tables 2 and 3 mimic an apparent anomaly in the trend toward a decrease of critical pressure with increasing primary alcohol chain length. Hexanol's critical pressure is greater than that of pentanol, resulting in a decrease in predicted molar volume. Hexanol also has an

anomalously large critical compressibility. Note that measured boundary condition factors for both DPB and HMS in hexanol also exhibit an anomaly in the trend toward lower value with increasing chain length. Though the measured anomaly is smaller than the anomaly in the m-DKS calculation, it does suggest that the modified DKS model has some merit. We suspect that the estimation methods tend to amplify this effect in calculated boundary condition factors.

Several trends are apparent from the measured and calculated boundary condition factors presented in Tables 2 and 3. First, the measured values for HMS are larger than the DPB values in similar solvents by nearly a factor of 3. Second, the m-DKS calculations are larger than the DKS calculations by several hundred percent. Third, the HMS measurements exceed those of the DKS and m-DKS predictions, while the measured DPB results are bracketed by their DKS and m-DKS predictions. Fourth, comparison of HMS and DPB predictions within each model indicate that similar results are expected in measured values of rotational diffusion times for HMS and DPB. In other words, comparison of the predicted boundary condition factors calculated by either the DKS or m-DKS methods demonstrates nearly identical results for HMS and DPB. We conclude that the quasihydrodynamic boundary condition factor cannot account for the experimentally observed difference between the HMS and DPB measurements. On the basis of these considerations, we conclude that the dramatic increase in the slope of the HMS measurements cannot be accounted for in terms of the influence of molecular size and shape alone. Comparison of the DPB measurements to the predicted boundary condition factor of 0.507 indicates that the DPB boundary condition is 40–60% below the slip prediction, whereas the measured HMS boundary condition is 30–60% below the stick prediction. This suggests that DPB is experiencing slip-like conditions while HMS is experiencing stick-like conditions due to attractive interaction between the hydroxyl group and the polar solvent. We now wish to explore the physical basis for this observation.

V. Dielectric Friction and Hydrogen Bonding

The fact that the HMS rotational diffusion times exceed measured and predicted values for a nonpolar solute such as DPB indicate that attractive solvent–solute interactions are at play. Waldeck and co-workers have observed similar effects in comparative studies of polar solutes in polar and nonpolar solvents and have attributed the difference to dielectric friction.^{3,4,14} Nee and Zwanzig presented a theory for dielectric friction, which predicts that rotational diffusion times should scale with solvent dielectric constant according to eq 1.²¹ The Nee–Zwanzig model treats the solvent as a dielectric continuum and the solute as a point dipole in a spherical cavity. Several recent improvements to this theory have been published. Hubbard and Wolynes⁴⁶ have examined the influence of frequency-dependent dielectric response on dielectric friction. Alavi and Waldeck^{2,3,5} have developed a model that treats the solute as an extended charge distribution within a spherical cavity and considers the position of the charges within the cavity surrounded by the continuum. In each of these models, the dependence of the rotational diffusion time on solvent dielectric constant remains the same in the zero frequency limit. This limit is appropriate for diffusive motion. Alavi and Waldeck have shown that the correction due to the finite dipole length is small as long as the length of the dipole is less than 25% of the cavity radius.⁵ In the case of HMS, the interacting solute dipole is fairly localized to the hydroxyl group and has an estimated length of 1.2 Å, and we anticipate a cavity radius on the order

of half the length of the long axis of the molecule. On the other hand, Alavi and Waldeck have shown that dielectric friction increases significantly for an ion of unit charge as it approaches the cavity boundary. In the case of neutral molecules, this effect scales with charge in a complex manner and its importance on dipoles located near the cavity boundary has not been examined. Alavi and Waldeck calculate dielectric friction from experimental data by first calculating the hydrodynamic friction using the SED equation and a slip boundary condition. However, several experimental studies including the present study have shown that boundary conditions are notoriously difficult to predict for polar solvents. One advantage of the investigation presented here is that DPB can be used to characterize the mechanical friction associated with a molecule having the same shape and size as HMS. In this manner, we avoid the need to estimate mechanical friction with hydrodynamic approximations.

We have chosen to examine the influence of dielectric friction on the rotational diffusion time of HMS using the Nee–Zwanzig model, eq 1, in our initial investigation of dielectric friction in hydrogen bonding solutes. Because we have measured the value of the HMS dipole moment, we can apply the Nee–Zwanzig model to our measurements using only a single adjustable parameter, ρ . Initial analysis based on the Nee–Zwanzig model will set the stage for a future study of the importance of solute charge distribution for polar solutes with relatively small dipole moments using the Alavi–Waldeck solute model. (The dipole model system examined by Alavi and Waldeck had a dipole moment of 4.8 D, whereas HMS has a measured dipole moment of 2.9 D.) The Alavi–Waldeck model represents an important refinement to the Nee–Zwanzig model and may result in a more accurate measure of the cavity radius.

The contribution of dielectric friction to rotational diffusion is included as an additive term in the rotational diffusion time expression

$$\tau_r = \tau_{\text{mech}} + \tau_{\text{DF}} \quad (3)$$

τ_{mech} is the contribution due to mechanical friction and is often characterized by the SED model. τ_{DF} is the contribution due to dielectric friction, and in this work, it is characterized by eq 1. Assuming that the hydroxyl moiety of HMS is responsible for the observed increase in the diffusion time, and that in its absence HMS would behave similarly to DPB, we model the HMS rotational diffusion time including dielectric friction as follows. We use the DPB data to predict the HMS rotational diffusion time in the absence of dielectric friction. This obviates the need to find the correct model for mechanical friction and is consistent with our observation that HMS and DPB have similar rotational diffusion times in non-hydrogen bonding solvents such as hexane and supercritical ethane. (See Table 1 and ref 17.) We then calculate the additive contribution of dielectric friction to the rotational diffusion time of HMS at a particular temperature using eq 1 as described below and add this to the DPB value at that temperature. This results in a predicted rotational diffusion time for HMS, and the prediction is compared with the value determined from the linear regression of the HMS data. (The linear regression is used because of slight differences in temperatures of HMS and DPB data.) Dielectric constants versus temperature for the solvents are taken from the literature.⁴⁷ Garg and Smyth have shown that alcohols in general exhibit three distinct Debye relaxation times.⁴⁷ The longest of these is associated with specific hydrogen bonding in the sense that it reflects overall rotational motion of molecules in a hydrogen-bonded cluster, which requires breaking of hydrogen bonds. Because the observed rotational diffusion times

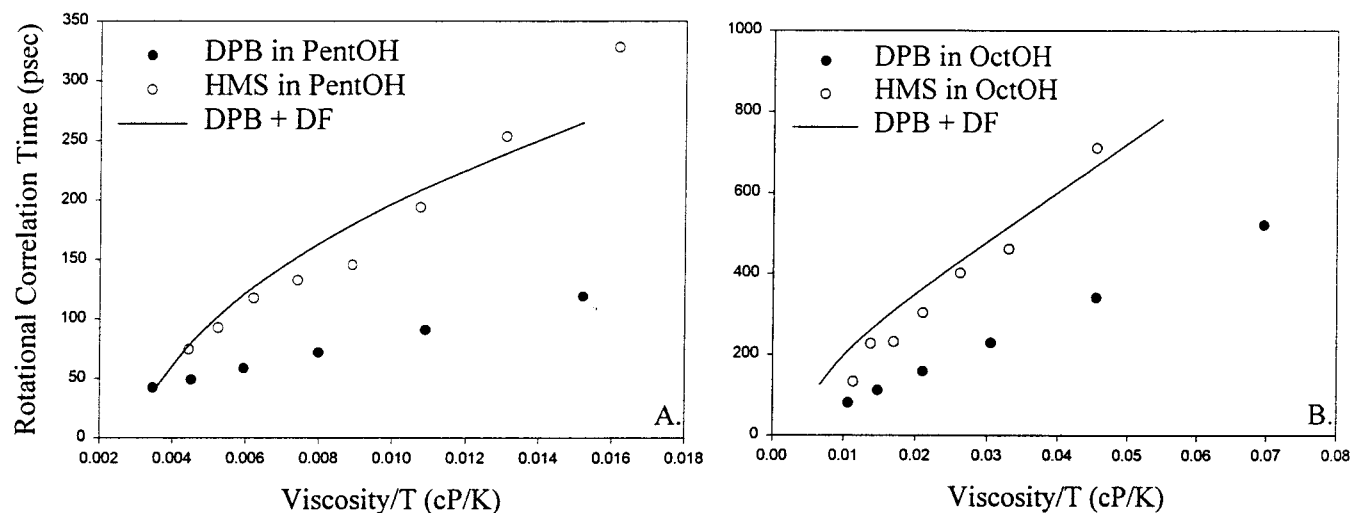


Figure 2. Comparison of measured HMS rotational diffusion times (open circles) with the sum of the measured DPB rotational diffusion times plus an additive dielectric friction contribution calculated using eq 1 (line). Results in (A) pentanol and (B) octanol are shown. Solid circles are the measured DPB rotational diffusion times. The agreement between the calculation and the HMS data is optimized by adjusting ρ , the cavity radius, in eq 1. Optimum values are given in Table 1.

TABLE 4: Parameters Used in the Analysis of HMS Dielectric Friction^a

alcohol	y intercept (ps)	slope (ps/°C)	ρ (Å)	cavity volume (Å ³)
propanol	580	-7.45	5.1	555
butanol	903	-12.4	5.3	623
pentanol	1234	-17.9	6.1	951
hexanol	1624	-24.2	5.5	696
heptanol	1965	-29.7	7.7	1912
octanol	2397	-37.7	8.8	2854

^a Slopes and y intercepts are linear regression results of Garg and Smith's Debye relaxation time vs temperature data. The ρ values minimize χ^2 for the HMS data compared with the sum of the DPB measured RDT plus an additive dielectric frictional contribution calculated using eq 1.

probe the diffusive solute rotational motion, we anticipate that the longest Debye relaxation time will be appropriate to model the observed behavior. The longest Debye relaxation times for propanol through octanol have been measured by Garg and Smith at three temperatures, and we use a linear regression fit of their results to estimate temperature-dependent Debye relaxation times for this analysis. Linear regression parameters for each solvent are given in Table 4. The dipole moment of HMS was measured as 2.9 ± 0.1 D using the apparatus and procedure described by Liu and Kauffman.⁴⁰ The remaining constant, ρ , is related to the solute volume in theory and is varied as a fitting parameter in this analysis. ρ is assumed to be temperature independent and constant for each particular solvent. Its value is adjusted to minimize the variance between model rotational diffusion times and the rotational diffusion times determined from the linear regression of the HMS data. Typical results are compared with the HMS data in Figure 2 for pentanol and octanol, and values of ρ that minimize the variance are tabulated in Table 4. The plot demonstrates qualitative agreement between the data and our method of analysis over a wide range of temperatures. Pronounced curvature in the predictions using eq 1 prevents complete quantitative agreement at all temperatures. Possible explanations for this observation are given in the following section.

VI. Discussion

The ρ values that give the best fit are intermediate between the radii associated with the long axis (length = 16.3 Å) and

the short axis (length = 4.93 Å) of HMS, indicating that the model is physically reasonable. We base this statement on the fact that ρ characterizes the volume of the solvent cavity, and in all cases the solvent cavity volume exceeds the van der Waals volume of the solute by at least a factor of 2 as shown in Table 4. The fact that the cavity radius is smaller than the long semi-axis of the molecule in some cases may reflect a reduced cavity volume due to distortion from a spherical shape, as would be expected on physical grounds. Application of the Alavi-Waldeck model may also result in a larger cavity radius. We observe a trend toward larger ρ values as the solvent size increases. It is tempting to attribute this observation to an increase in the effective cavity volume due to an increase in the free space per solvent molecule as the solvent volume increases with size. On the other hand, it is also true that as the value of ρ increases the contribution of the added dielectric friction term diminishes in the model. Thus, an increase in ρ with increasing aliphatic chain length may simply reflect a diminution of the effect of dielectric friction compared with mechanical friction. Regardless of the reason for this apparent trend, the Nee-Zwanzig equation can predict the difference between rotational diffusion times of HMS and DPB using reasonable values for ρ in the *n*-alcohols. Nee-Zwanzig theory predicts energy dissipation due to the phase lag between the rotation of a dipole in a spherical cavity and the solvent response. In the case of HMS, the solute dipole is localized on a hydrogen-bonding hydroxyl moiety and the solvent phase lag is interpreted as the result of solvent-solvent hydrogen bond breaking. Dielectric friction in this case is the result of attractive interactions between solvent and solute hydrogen bonding moieties, but is governed by the rotational motion of the solvent. An equally plausible, but mechanistically different interpretation views the increased friction as the result of direct hydrogen bonding between solvent and solute, and in this view we would conclude that the characteristic time for solvent-solute hydrogen bond breaking scales with the longest Debye relaxation time of the solvent. In this case, dielectric friction manifests itself as an increase in mechanical friction due to specific solvent attachment to the solute. Though we are unable to distinguish between these mechanisms in the present study, Kurnikova et al.^{33,34} have demonstrated the importance of the latter mechanism through molecular dynamics simulation. Regardless of the

mechanism, the present study clearly demonstrates that dielectric friction can be significant even when the solute is modestly polar. This is particularly evident by comparison of HMS with DPB and by comparison of hydrodynamic models for the pair of solutes as discussed in section III. It is clear that slight differences in mechanical properties of the solutes cannot account for the dramatic differences in the observed behavior of these two solutes. Friction due to hydrogen bonding between solvent and solute is a plausible explanation for the observation. The model calculations indicate that the predicted contribution of dielectric friction to the rotational diffusion time of HMS is consistent with the observed difference in rotational diffusion times of HMS and DPB in each solvent. We anticipate that improved agreement between our model and the HMS measurements can be realized with better characterization of the temperature dependence of the Debye relaxation time. Linear extrapolation of the Debye relaxation time versus temperature may represent a significant source of deviation between data and model. In particular, the notable curvature in the calculated contribution of dielectric friction may reflect an apparent curvature in temperature-dependent Debye relaxation times.⁴⁷ However, Debye relaxation times have only been reported at three temperatures,⁴⁷ and without more extensive data it is inappropriate to fit the data to higher order polynomials. Note also that it may be improper to assume ρ is constant with temperature since kinetic effects can influence the effective volume of solutes. Notwithstanding these deficiencies, we achieve agreement between the model and the HMS data using reasonable values for the cavity radius.

Acknowledgment. This research was supported by the National Science Foundation (CHE-9508744).

Supporting Information Available: Figures 1a–g and 2a–f. This material is available free of charge via the Internet at <http://pubs.acs.org>.

References and Notes

- Alavi, D. S.; Hartman, R. S.; Waldeck, D. H. *J. Chem. Phys.* **1990**, *92*, 4055.
- Alavi, D. S.; Waldeck, D. H. *J. Chem. Phys.* **1991**, *94*, 6196.
- Alavi, D. S.; Hartman, R. S.; Waldeck, D. H. *J. Chem. Phys.* **1991**, *95*, 6770.
- Alavi, D. S.; Hartman, R. S.; Waldeck, D. H. *J. Chem. Phys.* **1991**, *94*, 4509.
- Alavi, D. S.; Waldeck, D. H. *J. Chem. Phys.* **1993**, *98*, 3580.
- Anderton, R. M.; Kauffman, J. F. *J. Phys. Chem.* **1994**, *98*, 12117–12124.
- Anderton, R. M.; Kauffman, J. F. *J. Phys. Chem.* **1995**, *99*, 13759–13762.
- Ben-Amotz, D.; Scott, T. W. *J. Chem. Phys.* **1987**, *87*, 3739.
- Ben-Amotz, D.; Drake, J. M. *J. Chem. Phys.* **1988**, *89*, 1019.
- Courtney, S. H.; Kim, S. K.; Canonica, S.; Fleming, G. R. *J. Chem. Soc., Faraday Trans. 2* **1986**, *82*, 2065–2072.
- Evans, G. T.; Kivelson, D. *J. Chem. Phys.* **1986**, *84*, 385.
- Evans, G. T. *J. Chem. Phys.* **1988**, *88*, 5037.
- Dote, J. L.; Kivelson, D.; Schwartz, R. N. *J. Phys. Chem.* **1981**, *85*, 2169.
- Hartman, R. S.; Waldeck, D. H. *J. Phys. Chem.* **1994**, *98*, 1389–1393.
- Jiang, Y.; Blanchard, G. J. *J. Phys. Chem.* **1994**, *98*, 6436.
- Jonas, D. M.; Lang, M. J.; Nagasawa, Y.; Joo, T.; Fleming, G. R. *J. Phys. Chem.* **1996**, *100*, 12660–12673.
- Kauffman, J. F.; Wiemers, K.; Khajehpour, M. *Rev. High Pressure Sci. Technol.* **1998**, *7*, 1225.
- Kim, S. K.; Fleming, G. R. *J. Phys. Chem.* **1988**, *92*, 2168–2172.
- Lee, M.; Bain, A. J.; McCarthy, P. J.; Han, C. H.; Haseltine, J. N.; Smith, A. B., III; Hochstrasser, R. M. *J. Chem. Phys.* **1986**, *85*, 4341.
- Montgomery, M. E., Jr.; Green, M. A.; Wirth, M. J. *Anal. Chem.* **1992**, *64*, 1170–1175.
- Nee, T.-W.; Zwanzig, R. *J. Chem. Phys.* **1970**, *52*, 6353.
- Papazyan, A.; Maroncelli, M. *J. Chem. Phys.* **1995**, *102*, 2888–2919.
- Ravi, R.; Ben-Amotz, D. *Chem. Phys.* **1994**, *183*, 385–392.
- Ravichandran, S.; Perera, A.; Bagchi, B. *J. Chem. Phys.* **1997**, *107*, 8469.
- Roy, M.; Doraiswamy, S. *J. Chem. Phys.* **1993**, *98*, 3213.
- Schroeder, J.; Schwarzer, D.; Troe, J. *Ber. Bunsen-Ges. Phys. Chem.* **1990**, *94*, 1249.
- Temkin, S. I.; Steele, W. A. *J. Phys. Chem.* **1996**, *100*, 1996–2000.
- Van Konynenburg, P.; Steele, W. A. *J. Chem. Phys.* **1975**, *62*, 2301–2311.
- Zwanzig, R. *J. Chem. Phys.* **1963**, *38*, 1605.
- Hansen, J. P.; McDonald, I. R. *Theory of Simple Liquids*, 2nd ed.; Academic Press: New York, 1986.
- Gierer, A.; Wirtz, K. *Z. Naturforsch.* **1953**, *8*, 532.
- McQuarrie, D. A. *Statistical Mechanics*; Harper & Row: New York, 1977.
- Kurnikova, M. G.; Waldeck, D. H.; Coalson, R. D. *J. Chem. Phys.* **1996**, *105*, 628–638.
- Kurnikova, M. G.; Balabai, N.; Waldeck, D. H.; Coalson, R. D. *J. Am. Chem. Soc.* **1998**, *120*, 6121–6130.
- Bruehl, M.; Hynes, J. T. *J. Phys. Chem.* **1992**, *96*, 4068–4074.
- Lakowicz, J. R. *Principles of Fluorescence Spectroscopy*; Plenum Press: New York, 1983.
- Anderton, R. M.; Kauffman, J. F. *J. Phys. Chem.* **1994**, *98*, 12125–12132.
- Anderton, R. M.; Kauffman, J. F. *J. Phys. Chem.* **1995**, *99*, 14628–14631.
- Wiemers, K.; Kauffman, J. F. *J. Phys. Chem.*, to be submitted.
- Liu, C.; Kauffman, J. F. *Rev. Sci. Instrum.* **1996**, *67*, 525–529.
- Chen, G. S.; Liu, C.; Glaser, R.; Kauffman, J. F. *Chem. Commun. (Cambridge)* **1996**, 1719–1820.
- Bondi, A. *J. Phys. Chem.* **1964**, *68*, 441–451.
- Williams, A. M.; Jiang, Y.; Ben-Amotz, D. *Chem. Phys.* **1994**, *180*, 119–129.
- Hu, C. M.; Zwanzig, R. *J. Chem. Phys.* **1974**, *60*, 4354.
- Reid, R. C.; Prausnitz, J. M.; Poling, B. E. *The Properties of Gases and Liquids*; McGraw-Hill: New York, 1987.
- Hubbard, J. B.; Wolynes, P. G. *J. Chem. Phys.* **1978**, *69*, 998.
- Garg, S. K.; Smyth, C. P. *J. Phys. Chem.* **1965**, *69*, 1294.
- Strickler, S. J.; Berg, R. A. *J. Chem. Phys.* **1962**, *37*, 814.